AGU PUBLICATIONS

JGR

Journal of Geophysical Research: Space Physics

RESEARCH ARTICLE
10.1002/2016JA023766

Key Points:
- Global trajectories of ionospheric O^+ ions to the inner magnetosphere are traced
- Source regions of the energetic O^+ ions in the inner magnetosphere are identified
- We firstly calculate contributions of O^+ ions from several source regions to the ring current enhancement during substorm

Correspondence to:
Y. Nakayama,
yohei_nakayama@rish.kyoto-u.ac.jp

Citation:
Nakayama, Y., Y. Ebihara, M. C. Fok, and T. Tanaka (2017), Impact of substorm time O^+ outflow on ring current enhancement, *J. Geophys. Res. Space Physics*, *122*, 6304–6317, doi:10.1002/2016JA023766.

Received 5 DEC 2016
Accepted 23 MAY 2017
Accepted article online 26 MAY 2017
Published online 27 JUN 2017

Impact of substorm time O^+ outflow on ring current enhancement

Y. Nakayama[1], Y. Ebihara[1], M. C. Fok[2], and T. Tanaka[3]

[1]Research Institute for Sustainable Humanosphere, Kyoto University, Uji, Japan, [2]NASA Goddard Space Flight Space Center, Greenbelt, Maryland, USA, [3]International Center for Space Weather Science and Education, Kyushu University, Fukuoka, Japan

Abstract Energetic O^+ ions (tens of keV) rapidly increase in the inner magnetosphere and contribute significantly to the ring current during substorms. Previously, two source regions of the energetic O^+ ions have been proposed. The first one is the dayside polar region. Ions from the dayside polar region are transported to the lobe; then they are injected to the nightside plasma sheet during substorm expansion phase. The second one is the nightside aurora region. After the substorm onset, energetic O^+ ions are extracted from the ionosphere with the auroral acceleration processes, and the O^+ ions are directly supplied to the nightside plasma sheet. We investigated the relative importance of these two regions on supplying the energetic O^+ ions in the inner magnetosphere. We performed a test particle simulation in global MHD electromagnetic fields. We obtained the following results. (1) During the substorm growth phase, O^+ ions at tens of eV are extracted from the dayside polar region, resulting in the enhancement of the warm O^+ ions (hundreds of eV) in the lobe. After the substorm onset, the warm O^+ ions are nonadiabatically accelerated to tens of keV and injected to the inner magnetosphere. These O^+ ions contribute to most of the O^+ ring current. (2) O^+ ions at $<$ a few keVs are supplied from the nightside aurora region to the plasma sheet. However, their contribution to the O^+ ring current remains small. From the results, we concluded that the main source of the energetic O^+ ions is the dayside polar region.

1. Introduction

The ring current is populated by energetic particles (tens keV to a few hundreds of keV) such as H^+, O^+, He^+ ions, and electrons [*Gonzalez et al.*, 1994; *Daglis et al.*, 1999]. During quiet times, the ion pressure in the ring current region is dominated by H^+ ions [e.g., *Gloeckler et al.*, 1985; *Krimigis et al.*, 1985; *Hamilton et al.*, 1988]. However, the contribution of O^+ ions to the ring current becomes large with enhanced geomagnetic activity [e.g., *Lundin et al.*, 1980; *Hamilton et al.*, 1988; *Kistler et al.*, 1989; *Roeder et al.*, 1996; *Daglis*, 1997; *Daglis et al.*, 2000; *Feldstein et al.*, 2000; *Korth et al.*, 2000; *Greenspan and Hamilton*, 2002; *Nosé et al.*, 2005; *Kronberg et al.*, 2012]. It is accepted that the O^+ energization occurs on two different time scales: the storm time scale ($>$hours) and on the substorm time scale ($<$30 min) [*Keika et al.*, 2013].

During magnetic storms, convective transport is caused by the electric field induced into the magnetosphere under southward interplanetary magnetic field (IMF) through solar wind-magnetosphere-ionosphere coupling [e.g., *Ebihara and Ejiri*, 2000]. Accordingly, the energy density ratio of O^+/H^+ in the ring current region is increased [e.g., *Hamilton et al.*, 1988]. *Daglis* [1997], *Nosé et al.* [2005], and *Keika et al.* [2013] have shown that the ratio has a good correlation with magnetic storm strength represented by the *Dst* or *SYM-H* index. For intense storm events, O^+ ions become the dominant ion species [*Hamilton et al.*, 1988; *Daglis*, 1997; *Roeder et al.*, 1996; *Nosé et al.*, 2005].

During substorms, the energy flux of O^+ ions at tens of keV is rapidly increased in the inner magnetosphere [*Daglis and Axford*, 1996; *Nosé et al.*, 2000; *Fu et al.*, 2002]. Based on the Combined Release and Radiation Effects Satellite observation, *Fu et al.* [2002] analyzed rapid flux enhancements during around 400 substorm events under several types of ion composition. They showed that clear increases in the O^+ ion flux at $>$50 keV were identified in the nightside region in association with substorms. *Mitchell et al.* [2003] and *Keika et al.* [2010] examined global oxygen energetic neutral atom (ENA) data observed by the Imager for Magnetopause-to-Aurora Global Exploration/High Energy Neutral Atom (IMAGE/HENA). For some events, the oxygen ENA emitted from the energetic O^+ ions between ~50 and ~200 keV showed rapid enhancements almost simultaneously with the sudden brightening of aurora whereas that of hydrogen did not show clear increases.

To explain the enhancement of energetic O^+ ions during substorms, two processes have been proposed. The first one is the "nonadiabatic acceleration" process. O^+ ions from the dayside polar region are first transported to the lobe [*Vaisberg et al.*, 1995; *Moore et al.*, 1997]; then they are injected to the nightside plasma sheet and ring current region during substorm expansion phase undergoing nonadiabatic acceleration [e.g., *Nosé et al.*, 2000; *Fok et al.*, 2006; *Nakayama et al.*, 2015]. The second one is the "direct supply" process. Just after the substorm onset, energetic O^+ ions are extracted from the ionosphere with the auroral acceleration processes, and the O^+ ions are directly supplied to the nightside plasma sheet [e.g., *Gazey et al.*, 1996; *Sauvaud et al.*, 2004; *Ohtani et al.*, 2011; *Kistler et al.*, 2016]. To examine these processes, both observation and modeling studies have been conducted. *Mitchell et al.* [2003] investigated population of energetic O^+ ions through the bursts of oxygen ENA observed by IMAGE/HENA. They pointed out that the fast response (~20 min) of the O^+ burst in the inner magnetosphere to the substorm expansion onset is understood by the nonadiabatic acceleration in the near-Earth plasma sheet. *Fok et al.* [2006] traced global trajectories of ionospheric O^+ ions to the ring current region in a simulated substorm given by the Lyon-Fedder-Mobarry MHD simulation. From the test particle simulation result, they suggested that a sudden enhancement of oxygen ENA measured by IMAGE/HENA can be explained by the nonadiabatic energization rather than the direct supply from the ionosphere. Previously, *Nosé et al.* [2016] and *Keika et al.* [2016] investigated the magnetic field dipolarization in the inner magnetosphere and its associated ion flux variations, using the magnetic field and energetic ion flux data acquired by the Van Allen Probes. They showed that O^+ ions at $>$50 keV are impulsively enhanced in all pitch angle, which indicates that they are transported from the plasma sheet. They also showed that the field-aligned and energy-dispersed O^+ ions at 0.1–5 keV are enhanced simultaneously to the onset of the dipolarization.

Previously, a global MHD simulation developed by *Tanaka et al.* [2010] and *Tanaka* [2015] succeeded to demonstrate several observable features that emerge during a substorm such as the current system that can be interpreted as a current wedge [*Tanaka et al.*, 2010], dipolarization with the energetic particle injection [*Ebihara and Tanaka*, 2013], westward traveling surge [*Tanaka*, 2015; *Ebihara and Tanaka*, 2015], quiet arc [*Ebihara and Tanaka*, 2016], and the magnetic disturbance at auroral latitudes [*Tanaka et al.*, 2010] as well as magnetic equator [*Ebihara et al.*, 2014]. In this paper, we traced guiding centers of test particles in the electromagnetic fields provided by the global MHD simulation and investigated impacts of the two processes (nonadiabatic acceleration and direct supply) to the O^+ ring current enhancement in a short time scale ($<$~30 min). To simulate a substorm time variation of O^+ outflow, we launched O^+ ions from the topside ionosphere with initial parameters calculated by the same method introduced by *Fok et al.* [2006] but in the different MHD system. In addition, we traced a sufficient number of O^+ ions to reproduce distribution function with high energy and time resolution. For O^+ ions which transported to the inner magnetosphere by way of the lobe, we extended a study of *Nakayama et al.* [2015]. *Nakayama et al.* [2015] calculated the full motion of O^+ ions from the lobe region to the inner magnetosphere. The distribution function in the lobe was assumed to be a kappa distribution with constant parameters during the substorm. In this study, we calculated a subsequent change of the O^+ distribution in the lobe and simulated the flux enhancement in the inner magnetosphere using the result as the initial condition of the simulation of *Nakayama et al.* [2015].

2. Simulations

2.1. Global MHD Simulation

We used a global MHD simulation developed by *Tanaka et al.* [2010] and *Tanaka* [2015] to derive the electric and magnetic fields associated with a substorm and to determine initial parameters of test particles. The simulation solves the ideal MHD equations by applying a finite volume total variation diminishing scheme in a grid system based on a dodecahedron [*Moriguchi et al.*, 2008]. The inner boundary is located at 2.6 R_E and a dipole magnetic field is assumed inside of the boundary. In this study, the interplanetary magnetic field (IMF) is turned from (0, 2.5, 5.0) to (0, 2.5, −5.0) nT to trigger a substorm. At the same time, the solar wind speed was increased from 372 to 500 km/s. The solar wind density was set to a constant value of 5 cm^{-3}. All simulation settings, grid system, and ionospheric conductivities are the same as those used by *Ebihara et al.* [2014], *Ebihara and Tanaka* [2015] and *Nakayama et al.* [2015]. The simulation result showed that the calculated *AL* index is rapidly decreased after 57 min from an arrival of the southward IMF at the bow shock. The minimum *AL* reaches −800 nT [*Ebihara et al.*, 2014] for this setting. When the *AL* is decreased, the dawn to dusk electric

field is enhanced to ~13 mV/m at between ~6.5 R_E and ~11.5 R_E in longitudinally narrow regions in the premidnight and postmidnight [*Nakayama et al.*, 2015]. In this study, the onset of substorm expansion phase is defined as the moment at which the *AL* index suddenly decreases, and hereinafter referred to as $T = 0$ min.

2.2. Test Particle Simulation for O^+ Outflow

We traced O^+ ions' trajectories from the ionosphere in the time-varying global MHD electromagnetic fields by using the guiding center approximation. We released the O^+ ions by the same manner introduced by *Fok et al.* [2006]. Source region was set as the topside ionosphere at 1000 km altitude and between 60° and 90° latitude in both hemispheres. O^+ ions were launched from the source region every 1 min. Initial velocity was randomly given in the thermal energy ranges between 0 and 1 keV, pitch angle ranges between 0° and 90°, and gyrophase angle ranges between 0° and 360°. In total, around 100 billion test particles were traced from the source region. The thermal energy and parallel potential drop at their source positions were calculated by using the results from the MHD simulation as follows:

$$E_{\mathrm{th}}(\mathrm{eV}) = 0.1\ \ \mathrm{eV} + 1.6 S_{1\mathrm{K}}^{1.26} \tag{1}$$

$$\Phi_{||}(\mathrm{V}) = 1500(J_{||} - 0.2)^2 \ \ \text{if}\ \ J_{||} > 0.2\mu\mathrm{A/m}^2 \tag{2}$$

$$\Phi_{||}(\mathrm{V}) = 0 \quad \text{if} \quad J_{||} < 0.2\mu\mathrm{A/m}^2\,, \tag{3}$$

where $S_{1\mathrm{K}}$ is the global Joule heating in the ionosphere provided in mW/m^2 mapped to 1000 km altitude and $\Phi_{||}$ is the upward potential drop along the magnetic field line. The description of the ion heating shown in equation (1) is based on observational studies of *Strangeway et al.* [2005] and *Zheng et al.* [2005]. Following these studies, we took the two primary energy sources of ion outflow, soft electron precipitation, and dissipation of downward Poynting flux, into consideration. A relationship between the upward field-aligned current at the ionosphere and the parallel potential drop in equations (2) and (3) is estimated from the Knight-like relation introduced in *Lyons* [1981]. We used a smaller threshold current density of 0.2 μA/m^2 than the value of 0.33 μA/m^2 which is used in *Fok et al.* [2006].

Figure 1 shows the MHD parameters and the corresponding O^+ outflow parameters at 1000 km altitude at $T = -15$ min, 0 min, and 15 min (positive upward). Large-scale field-aligned currents (FACs), which are consistent with those known as regions 1 and 2 current systems [*Iijima and Potemra*, 1976], are clearly shown. During the growth phase (left column), the intensity of the upward FAC and downward FAC is increased to 0.2 μA/m^2 in the regions 1 and 2. E_{th} is large in the dayside polar region where midday part of region 1 FAC is increased and in the dawn-midnight sector at ~70 magnetic latitude (MLAT). Due to the upward region 1 FAC, potential drop is increased to 10 V at ~75 MLAT and at ~13–15 MLT. At the substorm onset (middle column), sudden intensification of upward FAC, which may be regarded as the initial brightening of one of the quiet arcs, emerges at ~67 MLAT and at ~23 MLT. The potential drop is increased to ~3 eV by primarily the initial brightening. E_{th} is increased in the broad region in the dawn-midnight sector at ~65–~70 MLAT. After the substorm onset (right column), FAC is increased to ~0.4 μA/m^2 in the dusk sector at ~70 MLAT. The value fairly agrees with typical observations by the Active Magnetosphere and Planetary Electrodynamics Response Experiment satellite [*Anderson et al.*, 2014].

High E_{th} and potential drop is established in the dusk-midnight at ~65–70 MLT and dawn-midnight sector at ~70 MLT, respectively.

By using the O^+ outflow parameters above, we calculated the real number of particles ΔN for ith test particle:

$$\Delta N_i = f_i \Delta^3 r_i \Delta^3 v_i, \tag{4}$$

where $\Delta^3 r_i$ and $\Delta^3 v_i$ are the volumes in configuration space and velocity space. Distribution function in the source region was slightly modified from the original Kappa distribution [*Vasyliunas*, 1968; *Summers and Thorne*, 1991] in this study, which is given as

$$f_i = \frac{n}{\pi^{3/2}{\theta_\kappa}^3} \frac{\Gamma(\kappa+1)}{\kappa^{3/2}\Gamma(\kappa-1/2)} \left(1 + \frac{\left(\mathbf{v} - \frac{\mathbf{B}}{B}\sqrt{2e\Phi_{||}/m}\right)^2}{\kappa{\theta_\kappa}^2}\right)^{-(\kappa+1)}. \tag{5}$$

and

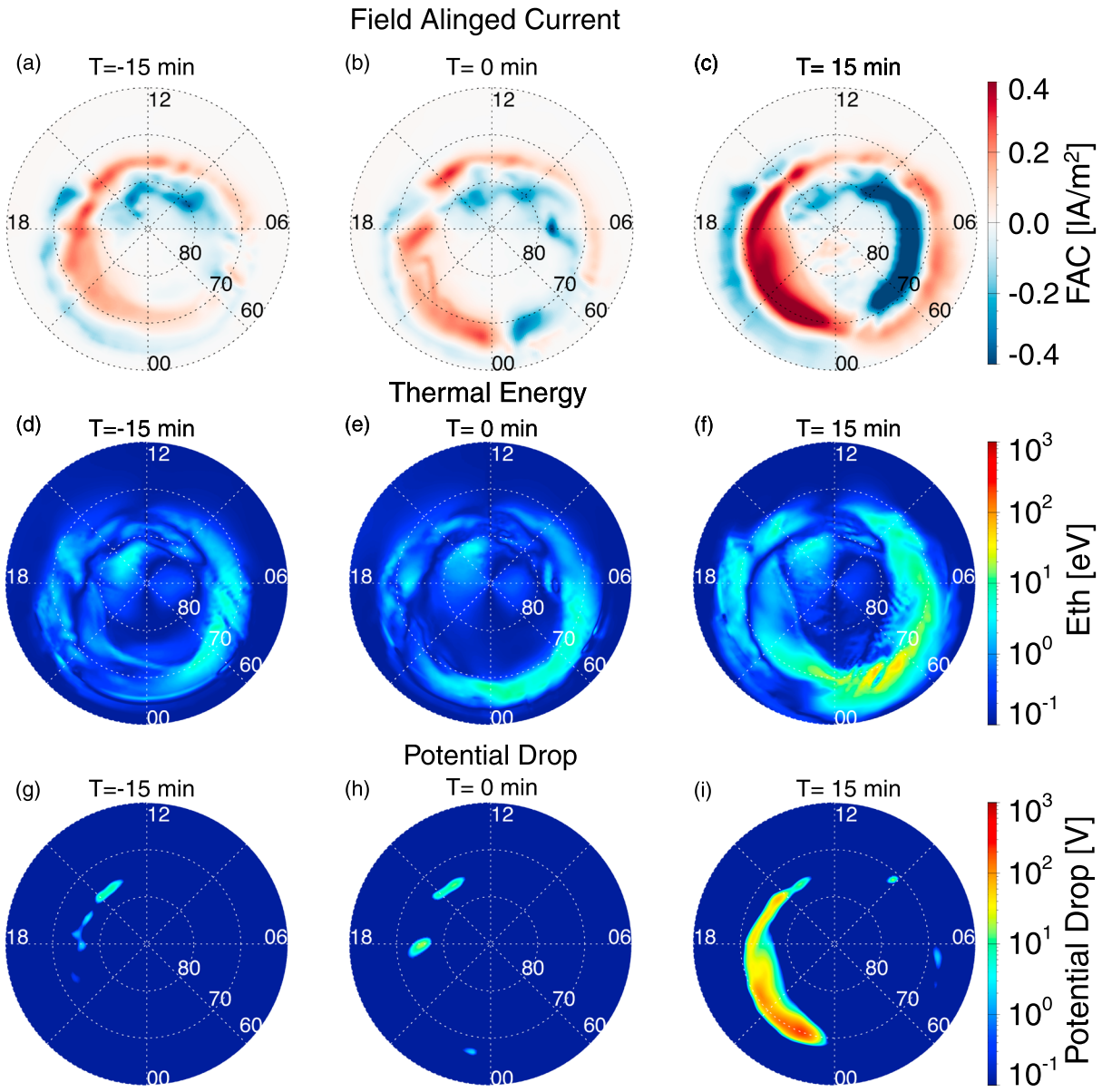

Figure 1. MHD conditions and auroral outflow parameters at 1000 km altitude at $T = -15$, 0, and 15 min.

$$\theta_\kappa = \frac{2\kappa - 3}{\kappa} \frac{E_{\mathrm{th}}}{m}, \tag{6}$$

where n, κ, k, m, and $\mathbf{v}$ are the density of O^+, the spectral index, the Boltzmann constant, the mass, and the velocity of O^+. In this study, the density n was assumed as n = 0.1 cm^{-3} based on *Ebihara et al.* [2006]. *Ebihara et al.* [2006] developed a statistical model of outflowing suprathermal ions from the long-term data from the suprathermal ion mass spectrometer on board the Akebono satellite. The model shows that an average of the number density of O^+ outflow is around 10^{-1} cm^{-3} under a solar minimum condition (the sunspot number is 20). In addition, we set the kappa parameter κ as 4.5. After tracing particles, the real numbers of test particles were summed up in small bins in the six-dimensional space, and the distribution function was calculated as

$$f = \frac{\Sigma \Delta N}{\Delta^3 r \Delta^3 v}. \tag{7}$$

Detailed calculations of the phase space mapping are explained in *Ebihara et al.* [2006] and *Nakayama et al.* [2015].

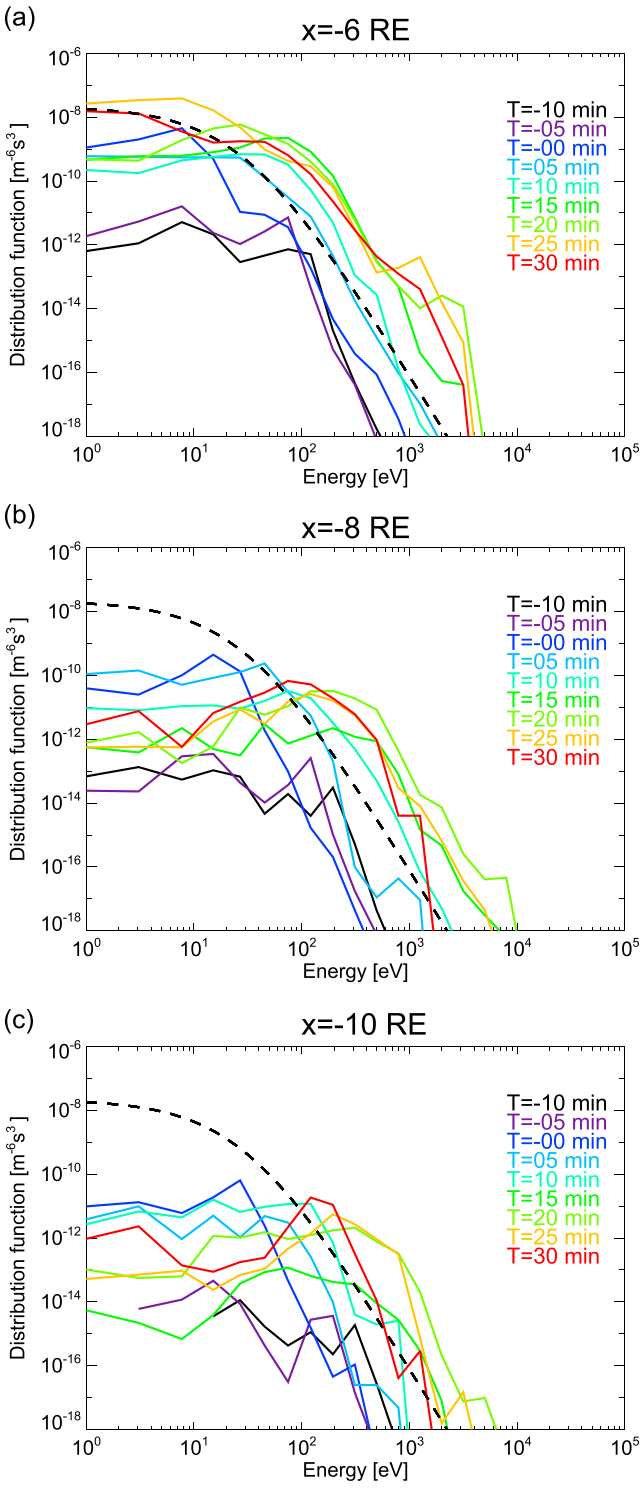

Figure 2. Temporal variations of the distribution function at (−6, 0, 2) R_E, (−8, 0, 2) R_E, and (−10, 0, 2) R_E, which located at plasma sheet, plasma sheet-lobe boundary, and plasma lobe, respectively. Black dashed line shows a Kappa distribution ($n = 0.1$ cm^{-3}, $\kappa = 4.5$, and $kT = 10$ eV), which is used as a distribution function of the O^+ ion flowing into the lobe region in *Nakayama et al.* [2015]. The distribution function is increased after the substorm onset, particularly, that in high-energy range (>100 eV) is significant.

3. Simulation Result

3.1. Substorm Time Variation of the O^+ Outflow

Figure 2 shows temporal variations of the distribution function at (−6, 0, 2) R_E, (−8, 0, 2) R_E, and (−10, 0, 2) R_E, which are located in the plasma sheet, near the plasma sheet-lobe boundary, and in the lobe, respectively. Black dashed line shows a kappa distribution which is used as a distribution function of the O^+ ion flowing into the lobe region in *Nakayama et al.* [2015]. Before the substorm onset, for all the three positions, the distribution function is almost flat at <100 eV, but the value abruptly decreases at >100 eV. The feature does not change before the substorm onset (before $T = -5$ min). After the substorm onset, the distribution function is increased at all energy. In particular, the increase at >100 eV is notable, and the value exceeds that of the kappa distribution (black dashed line). For example, at −10, 0, and 2 R_E, the distribution function is lower than 10^{-18} at 300 eV at $T = 0$ min, and the value increases by 6 orders (~10^{-12}) at $T = 20$ min.

We focused on the enhancement of the warm (>~300 eV) ions emerging at (−10, 0, 2) R_E and (−6, 0, 2) R_E after the substorm onset at $T = 20$ min. Figures 3a and 3b show launched positions of the warm ions. For the lobe ions, the main source is restricted in the dayside polar region (between 83 and 87 MLAT, and 12 MLT and 18 MLT). For the plasma sheet ions, there are two main source regions. The first one is found in a broad region in noon-dusk sector (between 70 and 90 MLAT, and 12 MLT and 18 MLT), and the second one is found in the nightside aurora region (between 65 and 70 MLAT, and 00 MLT and 01 MLT). Figures 3c–3f show the time of departure from the source and the initial energy of the lobe and plasma sheet ions. Black lines show the total

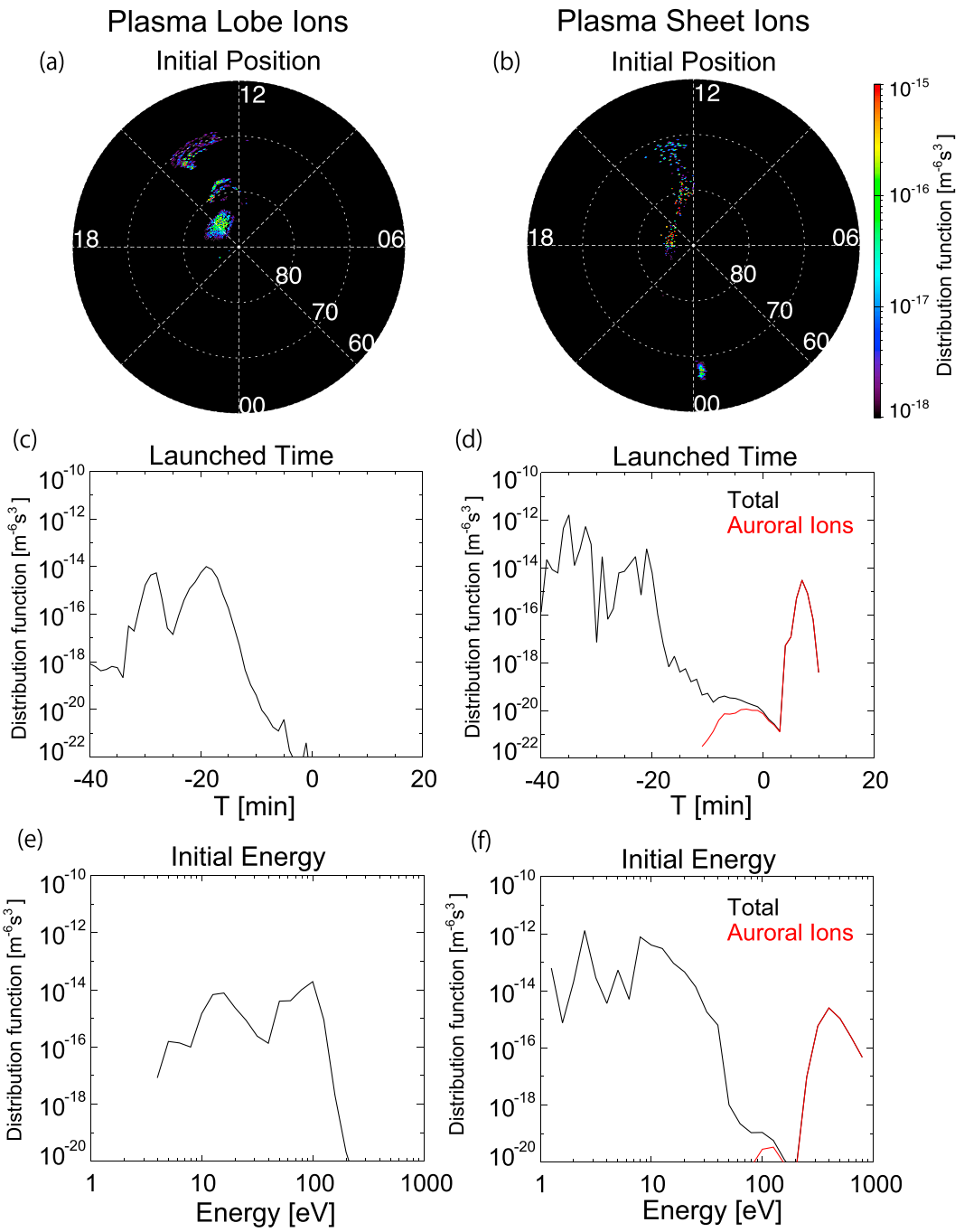

Figure 3. (a, b) Initial positions of the ions which flow into the lobe (at (−10, 0, 2) R_E) and the plasma sheet (at (−6, 0, 2) R_E) with >300 eV at T = 20 min. The distribution function as a function of (c, d) the time of departure from the source and (e, f) the initial energy.

value, and red lines show the value for the O^+ ion launched from the nightside aurora region. The lobe ions depart the dayside polar region with tens of eV (Figure 3e) during the substorm growth phase mainly between at T = −35 min and T = −10 min (Figure 3c). As shown in Figure 1d, O^+ ions from the dayside polar region are thermalized to ~10 eV due to the midday part of region 1 field-aligned current during the substorm growth phase. Therefore, a significant amount of O^+ ions at tens of eV are extracted from the region, results in the enhancement of the warm O^+ ions in the plasma lobe. The plasma sheet O^+ ions originated in the dayside region are launched during the substorm growth phase mainly between at

$T = -40$ min and $T = -20$ min (Figure 3d). Their initial energy is between 1 eV and 40 eV. Plasma sheet O^+ ions originated in the nightside aurora region are launched after the substorm onset (red line in Figure 3d). The initial energy is between 200 eV and 600 eV and it has a peak around at 400 eV. As shown in Figures 2e and 2f, the thermal energy in the nightside aurora region is increased (tens of eV) after the substorm onset due to the initial brightening of aurora. Although the thermal energy is increased only to tens of eV, the result indicates that a substantial amount of O^+ ions at hundreds of eV are directly supplied from the aurora region to the plasma sheet. In particular, the enhancement of plasma sheet O^+ ions at >1 keV is contributed only by the auroral O^+ ions (not shown).

Figure 4 shows trajectories and kinetic energy of the 20 typical test particles that flow from the dayside polar region into the vicinity of the point of -10, 0, and 2 R_E. The kinetic energy of the ions is indicated by color. Black circles in Figures 4a and 4b indicate the inner boundary of the global MHD simulation. Inside of the inner boundary, dipole magnetic field and no electric field are assumed. The O^+ ions depart at $T = -18$ to -17 min with initial energy of around 200 eV. After the departure, the O^+ ions move tailward and toward the equatorial plane. The kinetic energy is gradually increased from ~200 eV to ~400 eV. During the energy increase, the ions follow adiabatic motion because the energy is low (a few hundreds of eV), and magnetic field lines are not distorted before the substorm onset. Under the adiabatic motion, the energy gain of charged particle is given by

$$\frac{dK}{dt} = q\mathbf{V}\cdot\mathbf{E} + \mu\frac{\partial B}{\partial t},$$

where K, $\mathbf{V}$, $\mathbf{E}$, μ, and B are kinetic energy of the particle, velocity vector of the guiding center, electric field, magnetic moment, and magnetic field. Terms on the right-hand side are known as the gyrobetatron acceleration, and the drift betatron acceleration. Figure 4d shows energy gain rate of one typical O^+ ion of them. The red color indicates the energy gain rate due to the drift betatron, and the blue one indicates the energy gain rate due to the gyrobetatron. During the transport, the drift betatron contributes to the energy increase. This indicates that the O^+ ions are transported to the lobe region with the adiabatic acceleration under the influence of the large-scale convection electric field.

Figure 5 shows trajectories of the 20 typical test particles that contribute to the O^+ ions near the point of -6, 0, and 2 R_E. The O^+ ions are launched at $T = 7$–9 min with initial energy of at ~500–~1000 eV. After the departure, the O^+ ions move along the field line and flow into the vicinity of the point of -6, 0, and 2 R_E. During the transport, the kinetic energy is gradually increased and they gain ~200 eV. Again, the ion acceleration is due to the drift betatron and the gyrobetatron contributes little to it.

3.2. Flux Enhancement in the Inner Magnetosphere

The O^+ ions flow into the lobe region (Figure 2c) will be transported to the plasma sheet and ring current region with a significant acceleration due to the dawn to dusk electric field. The injection process is simulated by *Nakayama et al.* [2015], in which the same global MHD simulation result is used. In the simulation, O^+ ions were launched at $z = \pm 2$ R_E, ranging from $x = -7$ to -17 R_E and from $y = -10$ to 10 R_E. The distribution of the O^+ was assumed as a kappa distribution with constant parameters. In this paper, we used the result of the O^+ outflow simulation above (Figure 2) to specify the distribution function at the source plane of the injection simulation.

Figure 6 shows energy versus time spectrograms of the differential flux of the O^+ ions at fixed positions (at 6.0 R_E and at 00, 23, and 22 MLTs and in the equatorial plane). At 00 MALT, the flux increases almost simultaneously at all energies below 80 keV at $T = 0$ min, which is known as dispersionless structure [e.g., *Fu et al.*, 2002; *Keika et al.*, 2010; *Gkioulidou et al.*, 2015]. A lack of the energetic O^+ at <30 keV starting at $T = \sim 10$ min is called as a void structure [*Nakayama et al.*, 2016]. At 23 MLT, the flux enhancement appears first between ~80 keV and ~100 keV at $T = 1$ min and spreads to both higher and lower energies as time passes, which is known as a nose structure [*Smith and Hoffman*, 1974; *Ejiri et al.*, 1980]. At 22 MLT, the flux enhancement shows the similar structure at 23 MLT, but the energy time dispersion becomes more significant.

3.3. Contribution to the Ring Current

We investigated a magnetic perturbation on the Earth driven by the energetic O^+ ions enhanced in the inner magnetosphere. For the O^+ ions at the radial distance $r < 10$ R_E, we calculated the z component of $\Delta\mathbf{B}$ which is written by below:

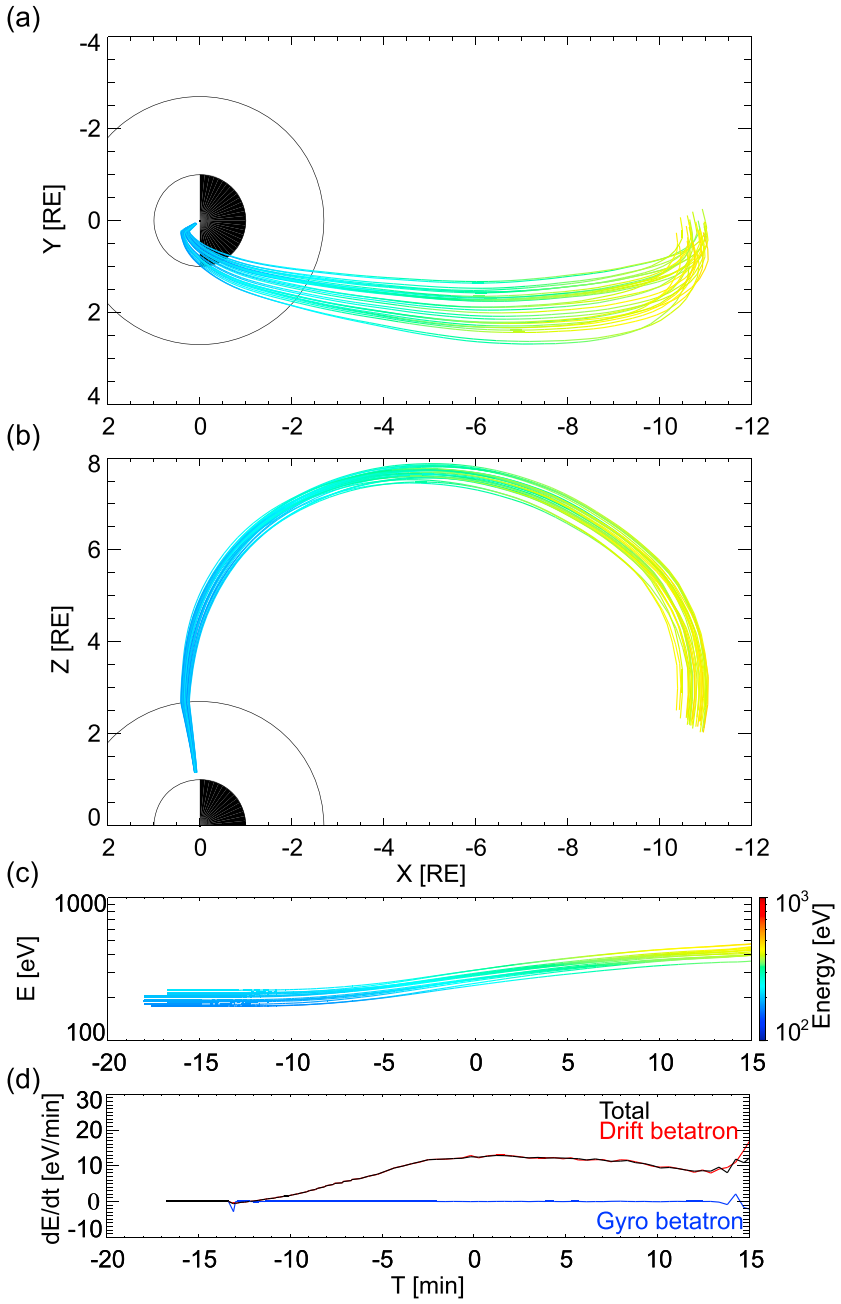

Figure 4. (a, b) Trajectories of the ions which flow into the lobe region from the dayside polar region, projected on the *x-y* and *x-z* plane. The kinetic energy of the ions is indicated by color. Black line indicates the inner boundary of the global MHD simulation. (c) Kinetic energy of the ions as a function of time. (d) Energy gain rate of one typical O^+ ion of them. The red color indicates the energy gain rate due to the drift betatron, and the blue one indicates the energy gain rate due to the gyrobetatron.

$$\Delta \mathbf{B} = -\sum \Delta N_i \frac{\mu_0 e \mathbf{v}}{4\pi} \times \frac{\mathbf{r}}{r^3},$$

where μ_0 is the magnetic permeability. Figure 7 shows the magnetic perturbation on the ground as a function of time. To clarify their source regions, we divided the O^+ ions to three groups. First group (Group A) consists of O^+ ions passed through the lobe region with >300 eV (red line) and second one (Group B) consists of those with <300 eV (blue line). Third group (Group C) consists of O^+ ions directly supplied from the nightside aurora region (green line). The total value (black line) starts to show a sharp decrease at T = ~10 min and has

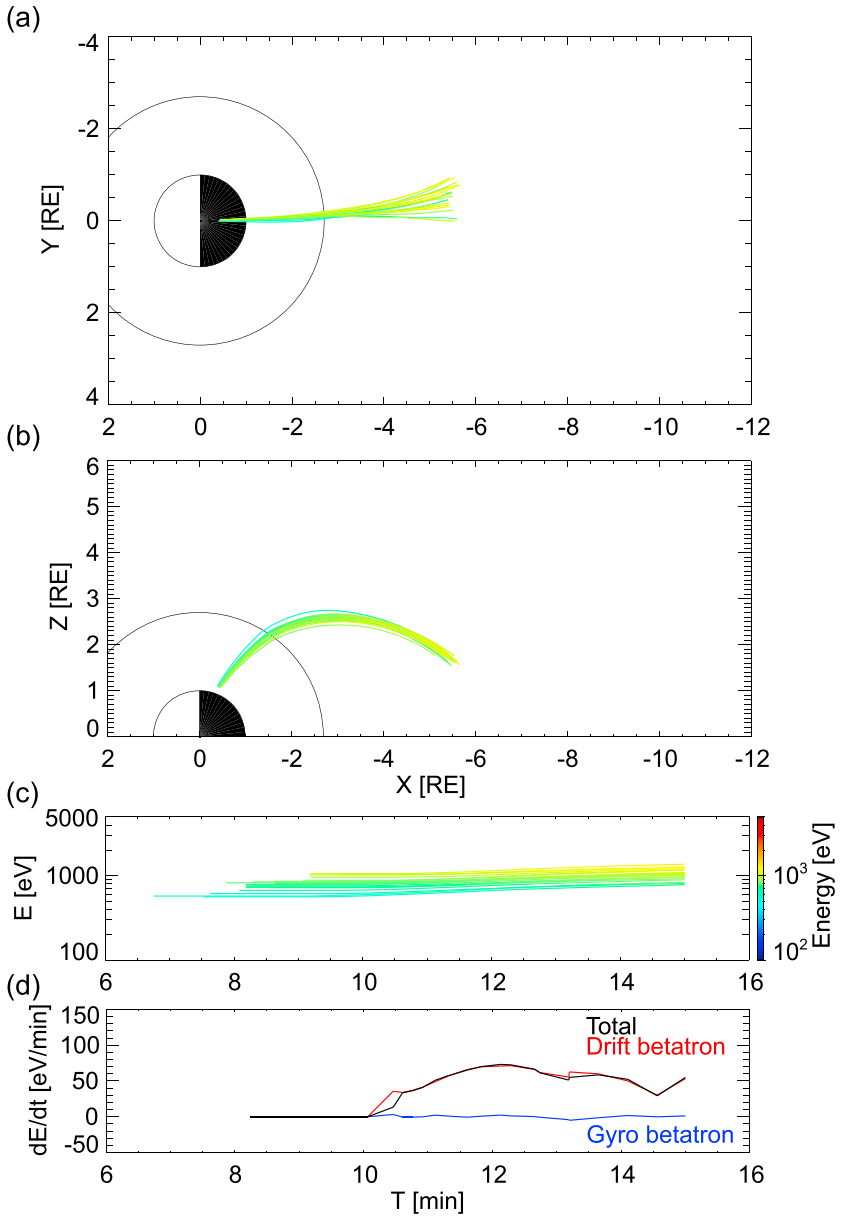

Figure 5. Same figure as Figure 4 for the O^+ ions, which are directly supplied to the plasma sheet from the night side aurora region.

two dips at $T = 17$ and 32 min. The minimum ΔB value is -7.2 nT at $T = 32$ min. Group A ions contribute most of the magnetic perturbation. For example, at $T = 32$ min, they decrease the Earth's magnetic field to -7.0 nT and the value reaches ~97% of total. Contributions of Groups B and C at the time are ~2% and ~1%, respectively. The result indicates that the enhancement of warm O^+ ions (hundreds of eV) in the lobe during substorm has a large impact on the ring current intensity.

4. Discussion

Observation studies reported an enhancement of the O^+ outflow during substorm growth phase. A statistical study by *Daglis and Axford* [1996] suggested that enhancements of O^+ outflow during the growth phase of substorms based on the O^+ measurements by Active Magnetospheric Particle Tracer Explorers/CCE. Some studies suggested that the enhancement takes place in the dayside polar region [e.g., *Moore et al.*, 1999;

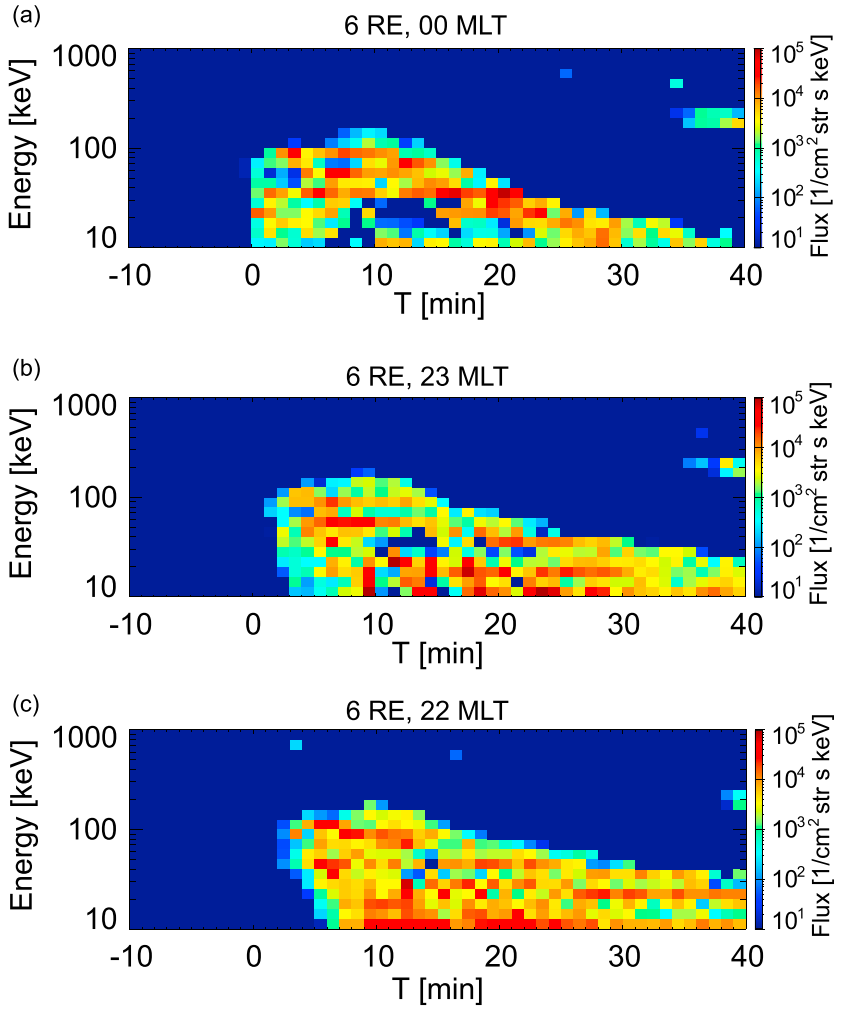

Figure 6. Energy versus time spectrograms of the differential flux of the O^+ ions at fixed positions (6.0 R_E; 00, 23, and 22 MLTs; the equatorial plane) simulated by the coupled simulation. The simulated flux shows rapid increase after substorm onset with a realistic dispersion.

Peroomian et al., 2006; *Zhang et al.*, 2011]. Our simulation result identified a specific region and a process of the enhancement. During the substorm growth phase, the midday part of region 1 FAC is increased (Figure 1a), resulting in the increase in the convection and Joule heating in the ionosphere. Consequently, the outflow of thermal O^+ ions (tens of eV) from this region is increased.

We also showed that the thermal O^+ ions from the dayside polar region are transported to the plasma lobe region in ~30 min (Figure 4). During the transport, the O^+ ions gain a few hundreds of eV due to the drift betatron acceleration. Accordingly, warm O^+ ions (hundreds of eV) are enhanced in the lobe region. This process works as a "preconditioning" of the O^+ ions transported to the inner magnetosphere with the nonadiabatic acceleration in the near-Earth neutral region. Some studies reported the preconditioning process on a storm time scale (a few hours). *Kistler et al.* [2010, 2016] showed that thermal O^+ ions originated in the cusp region are significantly enhanced in the near-Earth plasma sheet and the lobe on a storm time scale, and the O^+ ions enter the plasma sheet with the acceleration when reconnection occurs in the nightside region. Our simulation result suggests that the process can take places even in a short time scale (a substorm time scale).

On the other hand, some studies reported that O^+ ions at few hundreds of eV are extracted from the aurora region during substorms [*Sauvaud et al.*, 2004; *Andersson et al.*, 2005; *Moore et al.*, 2005; *Peroomian et al.*, 2006]. Our simulation result showed that after the substorm onset, the thermal energy in the nightside aurora region is increased due to the initial brightening of aurora. The thermal O^+ ions at hundreds of eV are

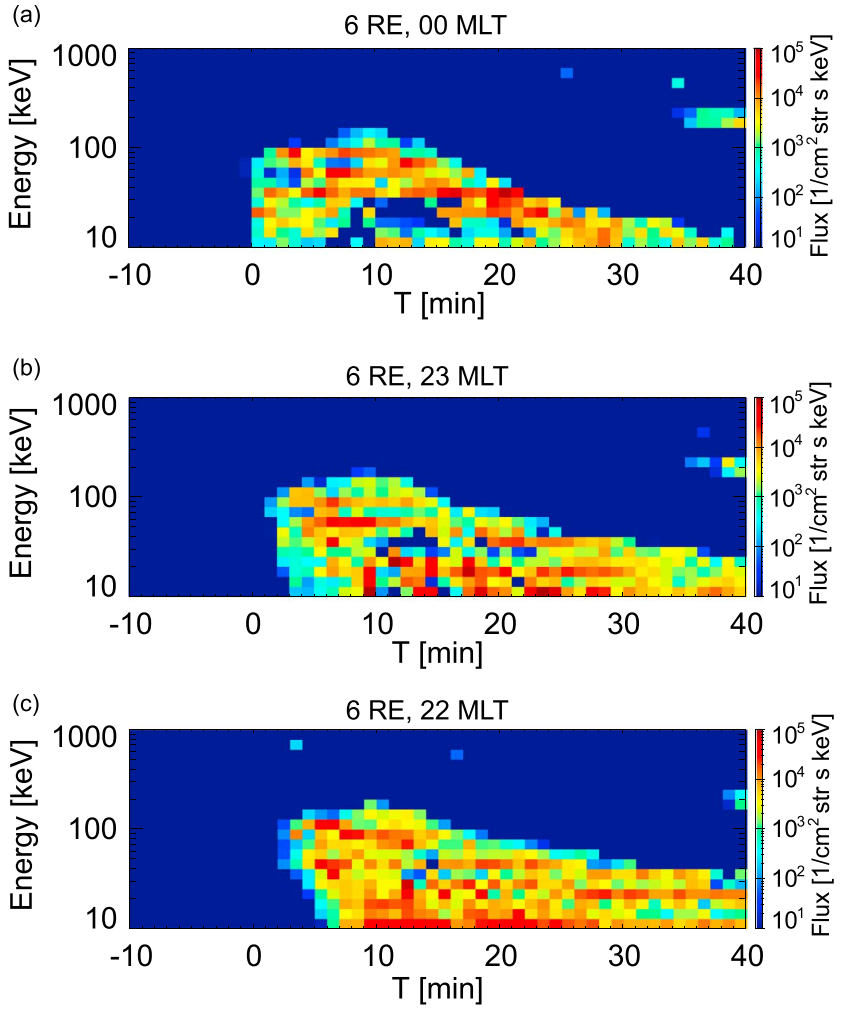

Figure 7. Magnetic perturbation on the ground due to the several groups of O^+ ion. The magnetic perturbation is induced after the substorm onset and reaches ~−7.2 nT at T = 32 min.

extracted from the region and directly supplied to the plasma sheet (Figure 4b). For auroral O^+ ions, a time delay between a substorm onset and an O^+ enhancement in the inner magnetosphere is known as an important factor. Many studies pointed out that the time delay is too short (<30 min) so that auroral O^+ ions extracted after the substorm onset cannot contribute to the enhancement [e.g., *Fu et al.*, 2002; *Mitchell et al.*, 2003]. However, previous Van Allen Probes observation revealed that O^+ ions at 0.1–10 keV in magnetic field-aligned directions are enhanced in a short time scale [*Keika et al.*, 2016; *Nosé et al.*, 2016]. *Nosé et al.* [2016] investigated their traveling time by a simple numerical calculation. They assumed the dipole magnetic field with no electric field and computed the transit time of O^+ ions from the ionosphere to the inner magnetosphere. The result showed that the auroral O^+ ion at ~1 keV reaches at L = 6 R_E and GMLAT = 15° in ~5 min. Our test particle simulation in the global MHD fields showed a similar result. The auroral O^+ ions with hundreds of eV can flow into the plasma sheet region in ~10 min (Figure 5). It suggests that the auroral O^+ ion is observable in the inner magnetosphere even in a short time scale. However, as we stated, their contribution to the ring current is small. This may be because their energy is low (< few keVs) compare with the O^+ ions accelerated by the dawn to dusk electric field.

We have calculated the magnetic perturbation induced by the O^+ ions from two different sources by using numerical simulations. Our simulation result showed that in a short time scale (<~30 min), the O^+ ring current is dominated by the O^+ ions originated in the dayside polar region. Particularly, the O^+ ions pass through the lobe region at >300 eV contribute most of the total O^+ ring current intensity. It indicates that an

enhancement of the warm O^+ ions in the lobe is a key phenomenon for the O^+ ring current enhancements often observed by in situ observations. On the other hand, the contribution of the auroral O^+ ions to the O^+ ring current is small in the short time scale from the beginning of the substorm expansion onset. However, it should be noted that the contribution may increases with additional acceleration processes. Some studies reported that the dipolarization is observed even in the inner magnetosphere ($<6\ R_E$) [*Ohtani et al.*, 2007; *Nosé et al.*, 2016]. The auroral O^+ ions supplied to $L < \sim 6\ R_E$ can be accelerated to tens of keV or a few hundreds of keV due to the local electric field induced by the dipolarization. On a long time scale, these ions (0.1–10 keV) can be further transported into the inner magnetosphere more easily than the injected high-energy O^+ ions ($> \sim 10$ keV) with an adiabatic acceleration due to the convection electric field. This is because the earthward $\mathbf{E} \times \mathbf{B}$ drift can be higher than the westward gradient and curvature drifts even in the deep inner magnetosphere. After the penetration due to the storm time convection electric field, the auroral O^+ ions may be a nonnegligible population to O^+ pressure and O^+ ring current. To simulate the storm time processes of the O^+ ions is our future study.

5. Conclusion

We traced O^+ ions from the ionosphere to the magnetosphere during a MHD substorm. We identified two source regions of lobe and plasma sheet plasmas. (1) During the substorm growth phase, O^+ ions at tens of eV are extracted from the dayside polar region. The O^+ ions convect to the lobe with the adiabatic acceleration, results in the enhancement of the warm O^+ ions (few hundreds of eV). After the substorm onset, the warm O^+ ions are nonadiabatically accelerated to tens of keV by the dawn to dusk electric field and injected to the inner magnetosphere. Finally, the ions contribute significantly to the ring current enhancement. (2) After the substorm onset, O^+ ions at hundreds of eV are extracted from the nightside aurora region, and they are directly supplied to the plasma sheet in a short time scale. However, their contribution to the ring current remains small.

Acknowledgments
Computation in the present study was performed with the KDK system of Research Institute for Sustainable Humanosphere (RISH) at Kyoto University as a collaborative research project. This study was supported by KAKENHI, Grant-in-Aid for Scientific Research (B) 15H03732. Data from MHD simulation are available on request (Y. Ebihara: ebihara@rish.kyoto-u.ac.jp).

References

Anderson, B. J., H. Korth, C. L. Waters, D. L. Green, V. G. Merkin, R. J. Barnes, and L. P. Dyrud (2014), Development of large-scale Birkeland currents determined from the Active Magnetosphere and Planetary Electrodynamics Response Experiment, *Geophys. Res. Lett.*, *41*, 3017–3025, doi:10.1002/2014GL059941.

Andersson, L., W. K. Peterson, and K. M. McBryde (2005), Estimates of the suprathermal O^+ outflow characteristic energy and relative location in the auroral oval, *Geophys. Res. Lett.*, *32*, L09104, doi:10.1029/2004GL021434.

Daglis, I. A. (1997), The role of magnetosphere-ionosphere coupling in magnetic storm dynamics, in *Magnetic Storms*, *Geophys. Monogr. Ser.*, vol. 98, edited by B. T. Tsurutani et al., pp. 107–116, AGU, Washington, D. C.

Daglis, I. A., and W. L. Axford (1996), Fast ionospheric response to enhanced activity in geospace: Ion feeding of the inner magnetotail, *J. Geophys. Res.*, *101*, 5047–5065, doi:10.1029/95JA02592.

Daglis, I. A., Y. Kamide, C. Mouikis, G. D. Reeves, E. T. Sarris, K. Shiokawa, and B. Wilken (2000), "Fine structure" of the storm-substorm relationship: Ion injections during *Dst* decrease, *Adv. Space Res.*, *25*(12), 2369–2372.

Daglis, L. A., R. M. Thorne, W. Baumjohann, and S. Orsini (1999), The terrestrial ring current: Origin, formation, and decay, *Rev. Geophys.*, *37*(4), 407–438.

Ebihara, Y., and M. Ejiri (2000), Simulation study on fundamental properties of the storm-time ring current, *J. Geophys. Res.*, *105*(A7), 15,843–15,859, doi:10.1029/1999JA900493.

Ebihara, Y., and T. Tanaka (2013), Fundamental properties of substorm-time energetic electrons in the inner magnetosphere, *J. Geophys. Res. Space Physics*, *118*, 1589–1603, doi:10.1002/jgra.50115.

Ebihara, Y., and T. Tanaka (2015), Substorm simulation: Formation of westward traveling surge, *J. Geophys. Res. Space Physics*, *120*, 10,466–10,484, doi:10.1002/2015JA021697.

Ebihara, Y., and T. Tanaka (2016), Substorm simulation: Quiet and N-S arcs preceding auroral breakup, *J. Geophys. Res. Space Physics*, *121*, 1201–1218, doi:10.1002/2015JA021831.

Ebihara, Y., M. Yamada, S. Watanabe, and M. Ejiri (2006), Fate of outflowing suprathermal oxygen ions that originate in the polar ionosphere, *J. Geophys. Res.*, *111*, A04219, doi:10.1029/2005JA011403.

Ebihara, Y., T. Tanaka, and T. Kikuchi (2014), Counter equatorial electrojet and overshielding after substorm onset: Global MHD simulation study, *J. Geophys. Res. Space Physics*, *119*, 7281–7296, doi:10.1002/2014JA020065.

Ejiri, M., R. Hoffman, and P. H. Smith (1980), Energetic particle penetrations into the inner magnetosphere, *J. Geophys. Res.*, *85*(A2), 653–663, doi:10.1029/JA085iA02p00653.

Feldstein, Y. I., L. A. Dremukhina, U. Mall, and J. Woch (2000), On the two-phase decay of the *Dst*-variation, *Geophys. Res. Lett.*, *27*(17), 2813–2816, doi:10.1029/2000GL003783.

Fok, M. C., T. E. Moore, P. C. Brandt, D. C. Delcourt, S. P. Slinker, and J. A. Fedder (2006), Impulsive enhancements of oxygen ions during substorms, *J. Geophys. Res.*, *111*, A10222, doi:10.1029/2006JA011839.

Fu, S. Y., Q. G. Zong, T. A. Fritz, Z. Y. Pu, and B. Wilken (2002), Composition signatures in ion injections and its dependence on geomagnetic conditions, *J. Geophys. Res.*, *107*(A10), 1299, doi:10.1029/2001JA002006.

Gazey, N. G. J., M. Lockwood, M. Grande, C. H. Perry, P. N. Smith, S. Coles, A. D. Aylward, R. J. Bunting, H. Opgenoorth, and B. Wilken (1996), EISCAT/CRRES observations: Nightside ionospheric ion outflow and oxygen-rich substorm injections, *Ann. Geophys.*, *14*(1), 1032–1043, doi:10.1007/s00585-996-1032-4.

Gkioulidou, M., et al. (2015), Spatial structure and temporal evolution of energetic particle injections in the inner magnetosphere during the 14 July 2013 substorm event, *J. Geophys. Res. Space Physics*, *120*, 1924–1938, doi:10.1002/2014JA020872.

Gloeckler, G., B. Wilken, W. Stuedemann, F. M. Ipavich, D. Hovestadt, D. C. Hamilton, and G. Kremser (1985), First composition measurement of the bulk of the storm-time ring current (1 to 300 keV/e) with AMPTECCE, *Geophys. Res. Lett.*, *12*(5), 325–328, doi:10.1029/GL012i005p00325.

Gonzalez, W. D., J. A. Joselyn, Y. Kamide, H. W. Kroehl, G. Rostoker, B. T. Tsurutani, and V. M. Vasyliunas (1994), What is a geomagnetic storm, *J. Geophys. Res.*, *99*, 5771–5792, doi:10.1029/93JA02867.

Greenspan, M. E., and D. C. Hamilton (2002), Relative contributions of H^+ and O^+ to the ring current energy near magnetic storm maximum, *J. Geophys. Res.*, *107*(A4), 1043, doi:10.1029/2001JA000155.

Hamilton, D. C., G. Gloeckler, F. M. Ipavich, W. Studemann, B. Wilken, and G. Kremser (1988), Ring current development during the great geomagnetic storm of February 1986, *J. Geophys. Res.*, *93*, 14,343–14,355.

Iijima, T., and T. A. Potemra (1976), The amplitude distribution of field-aligned currents at northern high latitudes observed by Triad, *J. Geophys. Res.*, *81*(13), 2165–2174, doi:10.1029/JA081i013p02165.

Keika, K., P. C. Brandt, S. Ohtani, D. G. Mitchell, K. Min, M. Nose, T. Obara, H. Koshiishi, and H. Matsumoto (2010), Mass-dependent evolution of energetic neutral atoms energy spectra during storm time substorms: Implication for O^+ nonadiabatic acceleration, *J. Geophys. Res.*, *115*, A00I12, doi:10.1029/2010JA015889.

Keika, K., L. M. Kistler, and P. C. Brandt (2013), Energization of O^+ ions in the Earth's inner magnetosphere and the effects on ring current buildup: A review of previous observations and possible mechanisms, *J. Geophys. Res. Space Physics*, *118*, 4441–4464, doi:10.1002/jgra.50371.

Keika, K., et al. (2016), Storm-time impulsive enhancements of energetic oxygen due to adiabatic acceleration of pre-existing warm oxygen in the inner magnetosphere, *J. Geophys. Res. Space Physics*, *120*, 7739–7752, doi:10.1002/2016JA022384.

Kistler, L. M., F. M. Ipavich, D. C. Hamilton, G. Gloeckler, B. Wilken, G. Kremser, and W. Stüdemann (1989), Energy spectra of the major ion species in the ring current during geomagnetic storms, *J. Geophys. Res.*, *94*(A4), 3579–3599, doi:10.1029/JA094iA04p03579.

Kistler, L. M., C. G. Mouikis, B. Klecker, and I. Dandouras (2010), Cusp as a source for oxygen in the plasma sheet during geomagnetic storms, *J. Geophys. Res.*, *115*, A03209, doi:10.1029/2009JA014838.

Kistler, L. M., et al. (2016), The source of O^+ in the storm time ring current, *J. Geophys. Res. Space Physics*, *121*, 5333–5349, doi:10.1002/2015JA022204.

Korth, A., R. H. W. Friedel, C. G. Mouikis, J. F. Fennell, J. R. Wygant, and H. Korth (2000), Comprehensive particle and field observations of magnetic storms at different local times from the CRRES spacecraft, *J. Geophys. Res.*, *105*(A8), 18,729–18,740, doi:10.1029/1999JA000430.

Krimigis, S. M., G. Gloeckler, R. W. Mcentire, T. A. Potemra, F. L. Scarf, and E. G. Shelley (1985), Magnetic storm of September 4, 1984: A synthesis of ring current spectra and energy densities measured with AMPTE/CCE, *Geophys. Res. Lett.*, *12*, 329–332, doi:10.1029/GL012i005p00329.

Kronberg, E. A., S. E. Haaland, P. W. Daly, E. E. Grigorenko, L. M. Kistler, M. Fränz, and I. Dandouras (2012), Oxygen and hydrogen ion abundance in the near-Earth magnetosphere: Statistical results on the response to the geomagnetic and solar wind activity conditions, *J. Geophys. Res.*, *117*, A12208, doi:10.1029/2012JA018071.

Lundin, R., L. R. Lyons, and N. Pissarenko (1980), Observations of the ring current composition at *L*, *Geophys. Res. Lett.*, *7*(6), 425–428, doi:10.1029/GL007i006p00425.

Lyons, L. R. (1981), The field-aligned current versus electric potential relation and auroral electrodynamics, in *Physics of Auroral Arc Formation*, *Geophys. Monogr. Ser.*, vol. 25, edited by S. I. Akasofu and J. R. Kan, pp. 252–259, AGU, Washington, D. C.

Mitchell, D. G., P. C. Brandt, E. C. Roelof, D. C. Hamilton, K. C. Retterer, and S. Mende (2003), Global imaging of O^+ from IMAGE/HENA, *Space Sci. Rev.*, *109*, 63–75.

Moore, T. E., et al. (1997), High-altitude observations of the polar wind, *Nature*, *277*, 349–351.

Moore, T. E., et al. (1999), Ionospheric mass ejection in response to a CME, *Geophys. Res. Lett.*, *26*, 2339–2342, doi:10.1029/1999GL900456.

Moore, T. E., M.-C. Fok, S. P. Christon, S.-H. Chen, M. O. Chandler, D. C. Delcourt, J. Fedder, S. Slinker, and M. Liemohn (2005), Solar and ionospheric plasmas in the ring current region, in *Inner Magnetosphere Interactions: New Perspectives from Imaging*, *Geophys. Monogr. Ser.*, vol. 159, edited by J. Burch et al., pp. 179–220, AGU, Washington, D. C.

Moriguchi, T., A. Nakamizo, T. Tanaka, T. Obara, and H. Shimazu (2008), Current systems in the Jovian magnetosphere, *J. Geophys. Res.*, *113*, A05204, doi:10.1029/2007JA012751.

Nakayama, Y., Y. Ebihara, and T. Tanaka (2015), Generation of large-amplitude electric field and subsequent enhancement of O^+ ion flux in the inner magnetosphere during substorms, *J. Geophys. Res. Space Physics*, *120*, 4825–4840, doi:10.1002/2015JA021309.

Nakayama, Y., Y. Ebihara, S. Ohtani, M. Gkioulidou, K. Takahashi, L. M. Kistler, and T. Tanaka (2016), Void structure of O^+ ions in the inner magnetosphere observed by the Van Allen Probes, *J. Geophys. Res. Space Physics*, *121*, 11,698–11,713, doi:10.1002/2016JA023013.

Nosé, M., S. Ohtani, A. T. Y. Lui, S. P. Christon, R. W. McEntire, D. J. Williams, T. Mukai, Y. Saito, and K. Yumoto (2000), Change of energetic ion composition in the plasma sheet during substorms, *J. Geophys. Res.*, *105*(A10), 23,277–23,286, doi:10.1029/2000JA000129.

Nosé, M., K. Takahashi, S. Ohtani, S. P. Christon, and R. W. McEntire (2005), Dynamics of ions of ionospheric origin during magnetic storms: Their acceleration mechanism and transport path to ring current, in *Physics and Modeling of the Inner Magnetosphere*, *Geophys. Monogr. Ser.*, vol. 155, edited by T. I. Pulkkinen, N. A. Tsyganenko, and R. H. W. Friedel, pp. 61–71, AGU, Washington, D. C.

Nosé, M., K. Keika, C. A. Kletzing, H. E. Spence, C. W. Smith, R. J. MacDowall, G. D. Reeves, B. A. Larsen, and D. G. Mitchell (2016), Van Allen Probes observations of magnetic field dipolarization and its associated O^+ flux variations in the inner magnetosphere at $L < 6.6$, *J. Geophys. Res. Space Physics*, *121*, 7572–7589, doi:10.1002/2016JA022549.

Ohtani, S., et al. (2007), Cluster observations in the magnetosphere during the 18 April 2002 sawtooth event: Dipolarization and injection at $r = 4.6\ R_E$, *J. Geophys. Res.*, *112*, A08213, doi:10.1029/2007JA012357.

Ohtani, S., M. Nosé, S. P. Christon, and A. T. Y. Lui (2011), Energetic O^+ and H^+ ions in the plasma sheet: Implications for the transport of ionospheric ions, *J. Geophys. Res.*, *116*, A10211, doi:10.1029/2011JA016532.

Peroomian, V., M. El-Alaoui, M. A. Abdalla, and L. M. Zelenyi (2006), Dynamics of ionospheric O^+ ions in the magnetosphere during the 24–25 September 1998 magnetic storm, *J. Geophys. Res.*, *111*, A12203, doi:10.1029/2006JA011790.

Roeder, J. L., J. F. Fennell, M. W. Chen, M. Schulz, M. Grande, and S. Livi (1996), CRRES observations of the composition of the ring-current ion populations, *Adv. Space Res.*, *17*(10), 17–24.

Sauvaud, J. A., et al. (2004), Case studies of the dynamics of ionospheric ions in the Earth's magnetotail, *J. Geophys. Res.*, *109*, A01212, doi:10.1029/2003JA009996.

Smith, P. H., and R. A. Hoffman (1974), Direct observation in the dusk hours of the characteristics of the storm time ring current particles during the beginning of magnetic storms, *J. Geophys. Res.*, *79*, 966–967, doi:10.1029/JA079i007p00966.

Strangeway, R. J., R. E. Ergun, Y.-J. Su, C. W. Carlson, and R. C. Elphic (2005), Factors controlling ionospheric outflows as observed at intermediate altitudes, *J. Geophys. Res.*, *110*, A03221, doi:10.1029/2004JA010829.

Summers, D., and M. Thorne (1991), The modified plasma dispersion function, *Phys. Plamas*, *3*, 1835, doi:10.1063/1.859653.1.

Tanaka, T. (2015), Substorm auroral dynamics reproduced by the advanced global M-I coupling simulation, in *Auroral Dynamics and Space Weather*, *Geophys. Monogr. Ser.*, vol. 215, edited by Y. Zhang and L. J. Paxton, pp. 177–192, AGU, Washington, D. C.

Tanaka, T., A. Nakamizo, A. Yoshikawa, S. Fujita, H. Shinagawa, H. Shimizu, T. Kikuchi, and K. K. Hashimoto (2010), Substorm convection and current system deduced from the global simulation, *J. Geophys. Res.*, *115*, A05220, doi:10.1029/JA014676.

Vaisberg, O. L., L. A. Avanov, J. L. Burch, and J. H. Waite (1995), Measurements of plasma in the magnetospheric tail lobes, *Adv. Space Res.*, *18*(8), 63.

Vasyliunas, V. M. (1968), A survey of low-energy electrons in the evening sector of the magnetosphere with OGO 1 and OGO 3, *J. Geophys. Res.*, *73*, 2839–2884, doi:10.1029/JA073i009p02839.

Zhang, J.-C., L. M. Kistler, C. G. Mouikis, H. Matsui, B. Klecker, I. Dandouras, and M. W. Dunlop (2011), Shock-driven variation in ionospheric outflow during the 11 October 2001 moderate storm, *J. Geophys. Res.*, *116*, A00J18, doi:10.1029/2010JA015627.

Zheng, Y., T. E. Moore, F. S. Mozer, C. T. Russell, and R. J. Strangeway (2005), Polar study of ionospheric ion outflow versus energy input, *J. Geophys. Res.*, *110*, A07210, doi:10.1029/2004JA010995.